Ibogaine induces juvenile-like plasticity and modulates functional and structural regulators of plasticity in the adult mouse visual cortex

Alejo Acuña
Universidad de la República
Federico Billeri
Scuola Normale Superiore
Valentino Totaro
Scuola Normale Superiore
Ignacio Carrera
Universidad de la República
Juan M. Mesa
Universidad de la República
Tommaso Pizzorusso
Scuola Normale Superiore
Francesco M. Rossi
fmrossi@fcien.edu.uy

Universidad de la República

Research Article

Keywords: Ibogaine, Visual Cortex, Experience-Dependent Plasticity, Monocular Deprivation, Behavioral Visual Acuity, Dendritic Spine Density, Perineuronal Nets, Parvalbuminergic Neurons, Vesicular GABA Transporter

Posted Date: December 18th, 2025

DOI: https://doi.org/10.21203/rs.3.rs-8387313/v1

Additional Declarations: No competing interests reported.

Abstract

Background: Psychedelics have emerged as powerful modulators of neural plasticity, yet whether the atypical psychedelic ibogaine can enhance plasticity remains poorly understood. Here, we investigated whether a single administration of ibogaine can reinstate juvenile-like experience-dependent plasticity in the adult mouse visual cortex, a canonical model for studying neuroplasticity.

Results: Adult mice were treated with ibogaine (40 mg/kg, i.p.) or vehicle, and 24 hours later subjected to 4 days of monocular deprivation (MD). Behavioral visual acuity was quantified using the optomotor response test, and structural plasticity was assessed through dendritic spine density analysis following Golgi staining. Ibogaine alone did not alter visual acuity or dendritic spine density in non-deprived adults. However, when coupled with MD, ibogaine restored youthful plasticity: MD significantly reduced visual acuity in the deprived eye and decreased dendritic spine density in the binocular visual cortex of ibogaine-treated, but not vehicle-treated, adult mice. To examine mechanistic correlates of these findings, we quantified perineuronal nets (PNNs), parvalbumin-positive interneurons (PVs), and inhibitory synaptic puncta labeled with the vesicular GABA transporter (vGAT). We found that ibogaine reduced PNN and PV staining intensity and density, decreased the proportion of PVs enwrapped by PNNs, and lowered vGAT-positive puncta density.

Conclusions: These results show that ibogaine re-establishes experience-dependent plasticity in the adult visual cortex and that this effect is accompanied by reductions in structural and inhibitory “brakes” on plasticity. Our findings suggest that ibogaine’s long-lasting therapeutic actions can arise, at least partially, from its ability to re-open windows of heightened cortical adaptability.

Background

Psychedelics are a large family of substances capable of profoundly altering perception, cognition and mood (1). Research on these substances has markedly accelerated over the past fifteen years, greatly due to accumulating clinical evidence showing their potential for the treatment of a wide range of mental disorders (1). For example, clinical trials have shown that psychedelics such as psilocybin and ketamine are beneficial in the treatment of Major Depressive Disorder (MDD), while Methylenedioxymethamphetamine (MDMA) is effective in the treatment of Post-Traumatic Stress Disorder (PTSD) (2,3,4,5).

Ibogaine is the main indole alkaloid derived from the root bark of the shrub *Tabernanthe iboga* and related plants of the Apocynaceae family (6,7). Traditionally, it is used in West-African religious, spiritual and healing ceremonies due to its psychedelic effects (6,7). In western culture, it initially gained attention after anecdotal reports claiming that its consumption had led people with SUDs to suddenly stop abusing substances (6,7). Following these reports a great deal of pre-clinical studies investigated into ibogaines’ putative anti-addictive properties, finding consistent effects on rodent models of substance abuse (8). Currently, a few observational studies and open label trials have found promising results in ibogaine for treating substance abuse (9, 10, 11, 12, see 13 for a review). Furthermore, other studies

have found it can reduce chronic disability related to Traumatic Brain Injury (TBI), as well as associated symptoms of post-traumatic stress disorder (PTSD), depression, anxiety and altered cognitive functioning (14, 15, 16). Nevertheless, ibogaine administration may induce cardiac arrhythmias due to blockade of the cardiac hERG potassium channel (17).

While most well-known psychedelics, such as Lysergic acid diethylamide (LSD) and psilocybin, are pharmacologically characterized as potent partial agonists of the 5HT2A serotonin receptor (18), ibogaine affinity to this receptor is low or negligible (19,20), affecting other molecular targets which has led to its classification as a non-classical (atypical) psychedelic (19,20). The subjective experience after ibogaine ingestion has also been reported to differ from that of classic (or serotonergic) psychedelics (21, 22). Users often describe it as a “waking dream”-like state; accordingly, a recent study on rats shows that ibogaine can induce a wakeful state with electrophysiological features resembling those of REM sleep (23).

The pharmacology of ibogaine, and its active metabolite noribogaine is complex, modulating with low potency interactions several types of molecular targets such as: ion channels (blockade of NMDA receptors)(24), monoamine transporters (mainly inhibition of SERT and VMAT2) (25), G protein coupled receptors (κ and μ opioid receptors among others) (26) and kinase signaling pathway potentiation (27). The term “matrix pharmacology” has recently been introduced to describe ibogaine’s ability to modulate multiple molecular targets and signaling pathways through modest-to-weak interactions (25). This contrasts with “polypharmacology,” which typically denotes potent agonism or antagonism at multiple targets (25).

Despite these differences, both ibogaine and classic psychedelics have been linked to enhanced neuroplasticity, i.e. the brain’s capacity to modify neural circuits. Ibogaine has been shown to increase the expression of Brain Derived Neurotrophic Factor (BDNF) and Glial cell Derived Neurotrophic Factor (GDNF) in both cortical and subcortical regions (28, 29), re-open a critical period for social rewards (30), and promote the expression of plasticity related genes (31). Furthermore, both ibogaine and its main metabolite, noribogaine, can increase dendritic spine density in cortical neurons *in vitro* (32,33).

Here, we investigated the effect of ibogaine on the mouse visual cortex, a model that has been used for decades to study the mechanisms regulating experience-dependent plasticity, and has allowed the discovery of several treatments that can enhance cortical plasticity in adult animals. Interestingly, several of these treatments are also known to have neurotherapeutic effects (34-38). Furthermore, critical period plasticity of the visual cortex has been recently proposed as a useful framework for studying the effects of psychedelics on neural plasticity (39).

Specifically, we focused on studying in adults two well reported plastic phenomena that are present only in juvenile mice during a period of heightened plasticity in the visual cortex (critical period), but that are absent during adulthood: (i) a reduction of dendritic spine density in the binocular visual cortex after monocular deprivation (MD) of the contralateral eye (40-43; but see also 44, 45); (ii) a reduction in visual

acuity of the deprived eye following MD (43, 46, 47). We found that, in both cases, adult mice treated with ibogaine show changes in response to MD that are characteristic of juvenile mice.

We then sought to investigate mechanistic correlates that might be enabling the plastic changes observed in ibogaine-treated adult mice. Global inhibition levels of a brain region, measured through different physiological and molecular techniques, are low during critical periods, and then increase during adulthood (48). Pharmacologically increasing inhibition during the critical period, results in a premature ending (49), while diminishing inhibition during adulthood, reopens juvenile-like plasticity (50). Thus, considering the role of inhibition as a brake for ocular dominance plasticity appearing on the end of critical periods, we studied perineuronal nets (PNNs) and parvalbuminergic neurons (PVs), which are largely colocalized (51), as well as the vesicular GABA transporter (vGAT) as an inhibitory synaptic marker (52). Importantly, it has been shown that PNNs finish maturing at the end of the critical period, and that their pharmacological removal in adulthood causes juvenile-like plasticity to be restored in the visual cortex (53), as well as in other brain regions (54). PV inhibitory neurons have been implicated in the regulation of critical periods and are considered of central importance in the regulation of brain plasticity (55-57).

Our results show that ibogaine administration reduces PNN and PV presence in the adult mouse visual cortex, with pronounced effects in layers IV and V, and also reduces vGAT levels.

Methods

Animals

All experiments were performed in accordance with the EC Directive 86/609/EEC for animal experiments (directive from the European Commission of the European Economic Community) and the Uruguayan Research Ethic Committees (protocol approval #1621, ExpFCien 240012-000026-22). A total of 42 C57BL6/J mice (both sexes) at postnatal (P) day 60 (P60) provided by the Unidad de Reactivos y Biomodelos de Experimentación, Facultad de Medicina, Universidad de la República, Montevideo, Uruguay, were used. Mice were bred under specific pathogen-free conditions, housed (6 per cage) in ventilated cages with positive pressure (20±1°C, relative humidity 40–60%, 14/10 h light-dark cycle), fed with standard mouse diet *ad libitum*, and had free access to water.

Ibogaine treatment

Ibogaine-HCl (IBO) was prepared in the Laboratorio de Síntesis Orgánica (Departamento de Química Orgánica, Facultad de Química) by decarboxylation of voacangine isolated from *Voacanga africana* root bark according to previously published method (28) (see **Suppl. material** and **Suppl. Table 1** for details). For administration to animals, ibogaine-HCl was dissolved at 4 mg/ml in EtOH 10%, and administered intraperitoneally (i.p.) at a dose of 40 mg/kg. Control animals were administered with vehicle (VEH; EtOH 10%).

Monocular deprivation

Monocular deprivation was performed 24 h after ibogaine administration, at P61, under ketamine-xylazine-acedan, 100-10-3 mg/Kg anesthesia. The eyelids of the right eye were sutured close as previously described (43), and kept this way for four days. The integrity of the suture was checked daily and mice were used only if the eyelids remained closed throughout the duration of the deprivation period. The eyelids were reopened the day before performing the optomotor test and the eye was checked to make sure it was not damaged.

Optomotor response test

Behavioral visual acuity was assessed using the Optomotor Response (OMR) test (43,59,60). Mice were put in an arena that consisted of four monitors arranged in a quadrangle (square, 35 cm side length), and two mirrors that were placed on top (roof) and on the bottom (floor) of the arena. The roof mirror had a central 5 cm diameter hole, where a camera was positioned to record the animal's behavior. This camera could be easily moved or removed to optimize positioning before the start of each recording session. A circular platform (height 13 cm, diameter 5 cm, distance from monitors 17.5 cm) was secured on the center of the bottom mirror, where the mouse was placed unrestrained. Stimuli were presented on the four monitors using the PsychoPy® software (PsychoPy v3.0) (61). The stimulus consisted of vertical sine-wave gratings drifting either clockwise or counterclockwise, with spatial frequency varying from trial to trial. Each trial presented gratings of a specific frequency moving clockwise for 30 s, followed by 30 s of counterclockwise motion, at a speed of 12°/s and 100% contrast. To maintain the animal's attention and facilitate faster testing, brief, salient luminance changes and light taps on the monitors were occasionally introduced during testing to prompt the animal to look toward the monitors. The spatial frequencies tested were: 0.1, 0.2, 0.3, 0.325, 0.35, 0.375, 0.4, 0.425, 0.45, and 0.8 cycles/degree (c/d). The 0.1 c/d frequency was always presented first, as it reliably evokes a response and therefore can be used as a control to confirm that the mouse is properly positioned and able to respond to the stimulus (59). The remaining frequencies were presented in random order to avoid potential confounding effects of time or fatigue on responses. Experiments were conducted under scarce light conditions (~12 cd/m²). All animals were habituated prior to testing through gentle handling and by being placed on the arena platform for 30 s to 1 min before stimulus presentation began. Videos were analyzed by quantifying head movements and comparing them to the direction of the stimulus. A head movement was counted as a response only if it matched both the direction and speed of the grating. Very short head movements and repositioning of the whole body were not counted as responses. Visual acuity was determined as the highest spatial frequency of the stimulus at which the mouse gave a response. After all mice had performed the optomotor test, they were sacrificed (by cervical dislocation) and their brains collected for Golgi staining.

Golgi staining

After removal, brains were rinsed in physiological solution and then Golgi-stained using the élite Golgi Kit (#006690, Bioenno, Tech, LLC), as previously described (43). Briefly, each brain was immersed in 5 ml of

an impregnation solution (provided with the kit), and stored at Room Temperature (RT) in darkness. The day after, the impregnation solution was renewed and the brains were kept inside it for 5 extra days at RT and darkness. After this, brains were cut with a vibratome (LeicaGeoSystems VT1000S) in 150 µm thick coronal slices, and the left visual cortex was collected in PB 0.1 M. Sections were incubated free-floating in the staining and clarity solutions (also provided with the kit), rinsed in PBST 0.01 M, directly mounted on gelatin-coated slides, and left to dry overnight. The following day slices were dehydrated in 95% and 100% EtOH subsequently, and then cleaned with xylene. Finally, slides were covered with coverslips using mounting media (Entellan, Sigma-Aldrich).

Spine density analysis

Photographs of the images were obtained using a D70S Digital Camera (Nikon) attached to a Microphot-FXA microscope (Research Microscope, Nikon) at 40x. In order to be used for quantification, slices had to have strongly stained neurons. Spine density quantification was performed on apical dendrites of pyramidal neurons in layers II-III and V of the binocular visual cortex (bVC). bVC position was determined by comparing sections at 4x, with images from the Paxinos and Franklin (2007) (62) mouse brain atlas (AP: between -4.36 and -3.08; ML: between +3.25 and +2.5). Only neurons showing typical pyramidal neuron morphology were analyzed (63, 64). In order to be quantified, dendrites had to meet the following criteria: (i) to be viewed clearly, without significant breaks or interrupted staining; (ii) not to be interrupted by other stained neurons; (iii) the soma had to be clearly identifiable and completely stained. Once dendrites were selected, the number of protrusions along the entire dendrite was counted. Image visualization and analysis was carried out with the free software Fiji (Fiji Is Just ImageJ, NIH).

Immunofluorescence staining

Mice were deeply anesthetized with ketamine-xylazine-acedan, 100-10-3 mg/Kg anesthesia and perfused via intracardiac infusion with cold PBS and then 4% paraformaldehyde (PFA, w/vol, in PBS). Brains were extracted and post-fixed overnight in PFA 4% in PBS at 4°C, then transferred to 30% (w/vol) sucrose in PBS for 48 h at 4°C. For each brain, 50 µm coronal sections spanning the whole visual cortex were collected free-floating in PBS, using a freezing microtome (Leica).

WFA and PV immunostaining

Sections were blocked at RT for 2 h in a solution containing 3% BSA (Sigma-Aldrich, A7906) in PBS, and then incubated o/n at 4°C with a solution containing biotinylated *Wisteria Floribunda* Lectin (WFA; Vector Laboratories, B-1355-2) 1:200 in blocking solution. Following PBS washes, sections were incubated in blocking solution containing 1:400 Streptavidin, Alexa Fluor™ 555 conjugate (Invitrogen, S21381), at RT for 2 h, and rinsed in PBS. Then slices were blocked in 10% BSA, 0.3% Triton X-100, PBS, for 1 h, washed in PBS and incubated o/n at 4°C with 1:400 mouse anti-Parvalbumin antibody (Sigma Aldrich, P3088), 1% BSA, 0.1% Triton X-100, in PBS. Then, sections were rinsed in PBS, incubated with 1:500 Goat anti-Mouse Alexa Fluor™ 488 (Invitrogen, A32723), 1% BSA, Triton X-100 0.1%, PBS, at RT for 2 h, and washed again

in PBS. Finally, sections were mounted on microscopy slides with VECTASHIELD® antifade mounting medium (Vector Laboratories, H-100), and stored at 4°C.

vGAT immunostaining

Slices were blocked at RT for 1 h in a solution containing 5% BSA, 0.3% Triton X-100, in PBS. Then, slices were incubated o/n at 4°C with a solution containing rabbit polyclonal anti-vesicular GABA transporter (vGAT; Synaptic Systems, 131003), 1:1000 in blocking solution. On the following day, sections were rinsed in PBS at RT and incubated with 1:400 Goat anti-Mouse Alexa Fluor™ 488 (Invitrogen, A32723) in blocking solution. Finally, sections were mounted on microscopy slides with VECTASHIELD® antifade mounting medium (Vector Laboratories, H-100), and stored at 4°C.

Image acquisition and quantification

Images were acquired using a Zeiss ApoTome.2 microscope and digitized by an AxioCam MR R3 12-bit camera. The acquisition software ZEN blue (RRID:SCR_013672) was used to control image acquisition.

WFA and PV

Sections stained with WFA and the anti-PV antibodies were imaged with a 10x objective. For the WFA channel, excitation light passed through a 538-562 nm bandpass filter and a 570 nm dichroic mirror, while emitted light was filtered with a 570-640 nm bandpass filter. For the PV channel, excitation light passed through a 450-490 nm bandpass filter and a 495 nm dichroic mirror, while emitted light passed through 500-550 nm bandpass. Exposure time was 225 ms for the WFA channel, and 1600 ms for the PV channel, while excitation light intensity was the same for all images. Each brain slice was obtained as a multi-image experiment on a single z-plane selected at the depth of maximal staining intensity. A tilted z-plane was acquired in order to reduce artifacts in image intensity that may arise if the tissue section is not sitting exactly perpendicular to the optical path. The angle of the z-plane was determined by linearly interpolating between 2-4 manually selected focus points. For all sections, 3 apotome images were acquired for optical sectioning. After the acquisition, multi-image tiles were stitched in ZEN and exported as 8-bit TIFF files for further processing.

X and Y coordinates of WFA staining and PV-immunolabeling were detected using a convolutional neural network (CNN) developed by (51), that was trained to detect PNNs and PV cells. After this, a binary mask delineating the visual cortex was manually drawn using the free software Fiji (Fiji Is Just ImageJ, NIH), and the number of PNNs and PVs falling within this mask was counted.

To analyze intensity, small image crops (50 × 50 pixels for PNNs, 25 x 25 for PVs) centered on the coordinates where the CNN detected PNN or PVs were obtained. Pixels belonging to the PNN or PV of each crop were detected using Otsu's binarization method. Intensity was defined as the average of the intensity values of all the pixels belonging to a PNN or PV.

Finally, “energy”, a metric that integrates both density and staining intensity of cells, was also estimated for both structures (51). Energy was calculated by summing the intensity of each PNN or PV in a cortical layer, and then dividing by the area of the layer. In this way energy is a metric that weighs the contribution of each structure to density, based on intensity.

We also assessed the co-localization of PNNs and PVs based on their (X, Y) positions in the original image. A PNN and a PV were considered co-localized if the distance between them was less than or equal to 15 pixels (9.675 µm). If multiple PVs or PNNs met this criterion for a given reference object, the closest one was selected as the co-localized counterpart. If no PV or PNN was within this distance, the reference object was classified as un-colocalized. Finally, we calculated the percentage of PV cells that were surrounded by a PNN (PNN+/PV cells, calculated as the ratio between colocalized PVs and total PVs), and the percentage of PNNs surrounding a PV cell (PV+/PNNs, calculated as the ratio between colocalized PNNs and total PNNs).

vGAT

A 63x oil immersion objective was used to image sections stained with the ant-vGAT antibody. Filters were the same as for PV imaging. For each section, serial optical sections at 0.33 µm intervals were imaged for a total of at least 15 optical sections (5 µm). Maximum intensity projections (MIPs) were generated from the group of 5 consecutive sections yielding the higher mean pixel intensity. Four separate pictures were taken from each slice (2 in superficial layers and 2 in deep layers). After the acquisition, images were exported as 8-bit TIFF files for further processing.

To identify vGAT positive puncta, images were first pre-processed. A 5-pixel mean filter was applied to each image, and the resulting output was multiplied by the original image to reduce background signal. To further enhance signal-to-noise ratio, a Gaussian filter with a sigma of 1.2 was applied to the new images, and the resulting blurred image was subtracted to it. Segmentation was then performed using the Otsu automatic thresholding method and puncta were detected and quantified using the Puncta Analyzer plug-in in the free software Fiji (Fiji Is Just ImageJ, NIH).

Statistical Analysis

The researcher was blind to both drug and MD treatment during all image acquisition steps, and also during quantification.

All data were analyzed using linear models, implemented in the lme4 package of RStudio (65, 66). For visual acuity analysis, a Linear Mixed Model (LMM) was used, in which visual acuity was entered as the dependent variable. Drug treatment (ibogaine or vehicle), monocular deprivation (absence or presence), and eye (left or right) were introduced as fixed effects. Subject identity was included as a random intercept.

WFA and PV measures (energy, intensity and density), PNN/PV colocalization density, and vGAT-positive puncta density, were also modeled with LMM. For each model, object density (or intensity or energy) was

introduced as the dependent variable, and drug treatment and layers as a fixed effect. In the case of PNN/PV colocalization density, layer was not included as a fixed effect, and instead object type (un-colocalized PNN, un-colocalized PV, colocalized structures) was included. Subject identity was included as a random intercept in all models.

Dendritic spine counts were modeled with a Generalized Linear Mixed Model (GLMM), of the Poisson family, with a logarithmic link function. Object count was introduced as the dependent variable, drug treatment and monocular deprivation as fixed effects, and neuron identity nested within subject identity was used as a random effect. The logarithm of dendritic segment length was included as an offset variable, to account for differences in counts due to varying segment lengths.

Finally, between group differences in the percentage of PNN+/PV cells and PV+/PNNs were analyzed separately, using a binary GLMM. The dependent variable was a binary variable, indicating if the structure (PNN or PV) was colocalized with its counterpart (PV or PNN, respectively) or not. Treatment and layer, as well as their interaction, were entered as fixed effect. Subject identity was entered as a random effect.

Wald Chi square tests were used to evaluate the significance of main effects and interactions in all models (implemented in the car package of RStudio, (67)). When post hoc tests were computed, Tukey's correction for multiple comparisons was applied (using the emmeans package in RStudio)

Results

In order to study whether ibogaine induces experience-dependent plasticity in the visual cortex of adult mice, we analyzed the effect of monocular deprivation on visual acuity, as a parameter of functional plasticity, and on dendritic spine density, as a parameter of structural plasticity.

Ibogaine restores functional plasticity in adult mice

First, we studied whether ibogaine by itself affects behavioral visual acuity (**Fig. 1**). Adult (P60) mice were treated with vehicle or ibogaine (40 mg/Kg) and 6 days later visual acuity was measured for both eyes separately with the optomotor response test (OMR). Our results show that ibogaine did not affect visual acuity of either eye, when comparing against the vehicle-treated group (χ^2_1=0.004, p=0.948). Additionally, visual acuity of the left (L) and right (R) eye was similar in animals treated with vehicle, as well as in animals treated with ibogaine (VEH L: 0.308±0.015 (c/d) vs. VEH R: 0.325±0.011 (c/d), n=6, t_{26}=-0.190, p=0.851; IBO L: 0.320±0.015 (c/d) vs. IBO R: 0.316±0.012 (c/d), n=6, t_{26}=-0.379, p=0.707).

Then, in order to study if ibogaine has an effect on experience-dependent plasticity, adult mice were treated with ibogaine or vehicle, and monocularly deprived for 4 days (right eye). Behavioral visual acuity was measured with the OMR test after reopening of the deprived eye (**Fig. 2**). Our results show that in ibogaine-treated mice, visual acuity of the right (R) deprived eye was reduced in comparison to the left (L) un-deprived eye (IBO L: 0.393±0.016 (c/d) vs. IBO R: 0.256±0.022 (c/d), n=8, t_{26}=7.221, p< 0.001). On

the contrary, visual acuity of R deprived and L un-deprived eye was similar in vehicle-treated mice (VEH L: 0.327±0.012 (c/d) vs. VEH R: 0.340±0.015, n=10, t_{26}=-0.734, p=0.469).

Ibogaine restores structural plasticity in adult mice

To study if ibogaine facilitates structural plasticity, we analyzed dendritic spine density on apical dendrites from pyramidal neurons of layer II-III and V of the left (contralateral to the deprived eye in MD mice) binocular visual cortex (**Fig. 3**). Following the optomotor test, adult mice of all groups were sacrificed and tissues processed with the Golgi staining method. Our results show that dendritic spine density was similar between vehicle- and ibogaine-treated adult animals (IBO: 0.825±0.049 (spines/µm), n=19 dendrites, n=3 mice, vs. VEH: 0.815±0.023 (spines/µm), n=13 dendrites, n=3 mice, z=0,331, p=0.987). However, following monocular deprivation, dendritic spine density was reduced in ibogaine-treated mice in comparison to vehicle-treated ones (IBO MD: 0.681±0.061 (spines/µm), n=14 dendrites, n=4 mice, vs. VEH MD: 0.827±0.040, n=32 dendrites, n=6 mice, z=-2.743, p=0.006).

Ibogaine reduces PNN/PV staining

Following treatment with vehicle or ibogaine, visual cortex sections of adult mice were processed by double-immunohistochemistry with the *Wisteria Floribunda* Lectin, as a marker of PNNs, and with the anti-Parvalbumin antibody as a marker of parvalbumin-positive neurons (PVs). We then calculated the “energy” of both structures, a single metric that integrates both density and staining intensity of cells. This metric, analogous to the one used by the Allen Institute gene expression dataset, has been used previously to analyze PNN and PV distribution (51). Our results show that PNN energy was diminished in the visual cortex of adult mice treated with ibogaine (**Fig. 4**), compared to mice treated with vehicle, although between group differences were marginally significant (IBO: 3220.410±3.902 (a.u.), n=6, vs. VEH: 5119.520±960.337 (a.u.), n=6, χ^2_1=-3.599, p=0.057).

In order to analyze whether the decrease in PNN staining observed in ibogaine-treated adult mice was selective of specific cortical layers, a layer analysis was done (**Table 1**). Results showed that PNN energy was mainly reduced in layer IV in ibogaine- vs. vehicle-treated mice (treatment by layer interaction, χ^2_4=-45.828). Since energy metrics are calculated taking into consideration density and intensity, we also analyzed these parameters separately in the whole visual cortex and through the different cortical layers. Results obtained with this analysis paralleled those obtained analyzing the energy parameter (**Suppl. Fig. 1** and **Suppl. Table 2** and **3**).

Table 1. Comparison of PNN energy across layers in the visual cortex of ibogaine- and vehicle-treated adult mice.			
L	**VEH**	**IBO**	**P**
I	310.057±73.691	193.761±28.598	0.205
II-III	1793.918±388.655	1065.854±163.678	0.495
IV	14073.726±2272.501	9243.356±1066.732	0.001
V	5459.219±1057.806	3587.312±467.124	0.105
VI	1655.734±295.329	1036.886±115.457	0.587

Table 1. PNN energy is reduced in layer IV of ibogaine treated mice. The table reports the values corresponding to PNN energy (mean±SEM) in the different layers (L) of the visual cortex of ibogaine- (IBO) and vehicle- (VEH) treated adult mice. P indicates the p values obtained comparing PNN energy of IBO and VEH mice between the same cortical layer.

Similarly, we found that parvalbumin energy (**Fig. 5**) was reduced in the visual cortex of ibogaine-treated adult mice as compared to vehicle treated mice (VEH: 11437.911±1882.036 (a.u.), n=6, vs. IBO: 5222.456±915.487 (a.u.), n=6, χ^2_1=9.087, p=0.002).

A layer specific analysis of PV energy indicated a treatment by layer interaction effect (χ^2_4=38.231, p<0.001). Between group comparisons showed PV staining was significantly reduced in ibogaine-treated mice in L2/3, L4 and L5 and (**Table 2**). Similarly to what we observed in PNNs, density and intensity results for PVs were similar to those obtained for PV energy (**Suppl. Fig. 2, Suppl. Table 4** and **5**).

Table 2. Comparison of PV energy across layers in the visual cortex of ibogaine- and vehicle-treated adult mice.			
L	**VEH**	**IBO**	**P**
I	995.501±221.511	671.052±148.051	0.727
II-III	9295.963±1810.578	7952.504±1533.515	0.042
IV	19074.523±3314.563	9295.963±1810.578	0.001
V	15366.794±2688.356	7506.193±1235.996	0.004
VI	5749.268±936.381	2690.310±485.116	0.146

Table 2. PV energy is reduced in cortical layers of ibogaine treated mice. The table reports the values corresponding to PV energy (mean±SEM) in the different layers (L) of the visual cortex of ibogaine- (IBO) and vehicle- (VEH) treated adult mice. P indicates the p values obtained comparing PV energy of IBO and VEH mice between the same cortical layer.

To explore if ibogaine affected the relationship between PNNs and PV cells in the visual cortex, we calculated the percentage of PV cells that were surrounded by PNNs (PNN+/PV cells) and the percentage of PNNs surrounding PV cells (PV+/PNNs) (**Fig. 6**). We found that the percentage of both PNN+/PV cells and PV+/PNNs were reduced in ibogaine treated mice (PNN+/PV cells: VEH: 31.178.±2.198%, n=6, vs. IBO: 37.431±2.992%, n=6, χ^2_1=4.739, p=0.029; PV+/PNNs: VEH: 66.326.±4.907%, n=6, vs. IBO: 47.665±4.723%, n=6, χ^2_1=7.146, p=0.007).

To further understand this result we looked at between-group differences in the density of colocalized and un-colocalized structures (**Suppl. Fig. 3**). We found that ibogaine reduced both the density of colocalized structures and PV+ cells that were not colocalized with PNNs, but the density of un-colocalized PNNs remained the same (un-colocalized PNN density: VEH: 29.977±6.260 (PNNs/mm^2), n=6, vs. IBO: 35.538±5.800 (PNNs/mm^2), n=6, t=0.274, p=0.786; un-colocalized PV density: VEH: 97.568±12.44 (PVs/mm^2), n=6, vs. IBO: 68.661±5.635 (PVs/mm^2), n=6, t=3.286, p=0.003; colocalized PNNs/PVs: VEH: 58.668±5.201 (PNNs/PVs/mm^2), n=6, vs. IBO: 32.972±3.107 (PNNs/PVs/mm^2), n=6, t=3.885, p<0.001). Overall, these results show that ibogaine by itself could set the ground for enhanced plasticity by reducing PNN and PV energy, as well as their co-localization.

Ibogaine reduces vGAT staining

Finally, we were interested in investigating if ibogaine affects the expression of the vesicular GABA transporter, vGAT (**Fig. 7**). We observed that the density of vGAT positive puncta was reduced in the visual cortex of adult mice treated with ibogaine, compared to vehicle treated animals (IBO: 0.552±0.020 (puncta/μm^2), n=6, vs. VEH: 0.657±0.039 (puncta/μm^2), n=6, χ^2_1=5.644, p=0.017).

Analysis of the mean size particle showed no difference between vehicle- and ibogaine-treated mice (VEH: 0.0624±0.0010 mm^2, n=6, vs. IBO: 0.0642±0.0005 mm^2, n=6, χ^2_1=0.432, p=0.510). Thus ibogaine also affects inhibitory neurons at the synaptic level, by reducing vGAT puncta density.

Discussion

Our results show that ibogaine can enhance plasticity in the adult mouse visual cortex. Specifically, we showed that a protocol of monocular deprivation, that usually does not induce changes in adult mice, reduces visual acuity of the deprived eye, as well as dendritic spine density in the binocular visual cortex contralateral to the deprived eye, only when coupled with ibogaine treatment. Furthermore, we found that ibogaine administration correlates with a reduction in perineuronal nets, parvalbumin-positive interneurons, and vesicular GABA transporter (vGAT), all factors that are known brakes of cortical plasticity.

To estimate visual acuity, we used the optomotor response (OMR) test (59). It has been previously shown that the OMR is a useful tool to detect experience-dependent plastic changes in visual acuity: MD induces a decrease of visual acuity of the deprived eye of young mice during the critical period for ocular

dominance plasticity, but not during adulthood (43, 46, 47). Here we showed that ibogaine treatment in adult mice restores sensitivity to MD, detected as a decrease in visual acuity of the deprived eye, indicating that ibogaine can restore juvenile-like plasticity levels.

Then, to study plasticity at a morphological level we analyzed dendritic spine density by using Golgi-like staining and counting all protrusions along dendrites of LII-III and V pyramidal neurons. Other works have shown that MD during the critical period reduce dendritic spine density in the contralateral visual cortex of the deprived eye (40-43; but see also 44, 45). Similar to visual acuity, we found that changes in ibogaine treated MD mice mimic those found in critical period MD mice, reasserting that ibogaine restores plasticity in the visual cortex.

Interestingly, ibogaine *per se* did not induce effects on visual acuity nor on dendritic spine density but only when coupled to MD, reasserting that it potentiates experience-dependent plasticity. Other studies have found that ibogaine, or its main metabolite noribogaine, increases dendritic spine density in cortical neurons (32, 33). Importantly, the *in vitro* nature of those experiments limits the extent to which they can be directly compared with our *in vivo* results.

An important feature of our study is that visual experience manipulation by MD was performed 24 h after ibogaine administration, when both the drug and its main metabolite have been cleared off the rodent's body (68). This indicates that the potential for plastic changes outlasts pharmacokinetic elimination of the drug and its metabolite. Long-lasting effects of ibogaine administration on behavioral and molecular markers of plasticity have also been observed in other experimental models (29,30).

As for the mechanisms underlying the plasticity-inducing effects of ibogaine, we focused on the analysis of markers of the two main factors controlling the opening, duration and closure of the critical period and plasticity levels: the inhibitory tone and the maturation of structural brakes (48, 54, 69). Our results show that ibogaine treatment in adult mice induces a decrease in PV, PNN, and the colocalized PV/PNN structures, as well as vGAT, indicating an effect on both structural and inhibitory limiting factors. The observation that there are more PV neurons lacking PNNs following ibogaine treatment agrees with the plasticity-inducing effect of ibogaine. It is considered that when PNN surrounding PVs are reduced or absent, PV neurons exhibit increased plasticity due to modulation of their synaptic properties and network oscillations (70, 71). A reduction in vGAT staining has been observed also following other strategies that, like ibogaine, potentiate plasticity in the visual cortex of adult mice, such as fluoxetine treatment and enriched environment (72, 73).

Finally, it is worth noting that our results show that, even though ibogaine has a complex pharmacology that differs with respect to other psychedelics, it shares the ability to re-open a period of juvenile-like plasticity. For example, it has been shown that both ketamine (35, 74-76) and LSD (77) also increase experience-dependent plasticity in the visual cortex. A complementary finding is that both of these drugs, along with ibogaine, psilocybin and MDMA re-open a critical period of social reward learning (30). Furthermore, both changes in parvalbumin positive cells and PNNs have been found after the administration of psilocybin, MDMA, ketamine and LSD (30, 76, 78-80), and psychedelic modulation of

critical periods is associated with extensive remodeling of extracellular-matrix gene transcription (30). Therefore, as suggested previously (30, 81), it seems that despite diverse mechanisms of action, psychedelics, as a class, share the property of increasing plasticity while altering factors that include both structural and functional changes related to the remodeling of PNNs and PVs respectively.

A limitation of the present study is that it does not delve into the pharmacological mechanisms behind the plasticity-inducing effect of ibogaine. Given ibogaine's complex pharmacology, this is a difficult task, with several possibilities. It has been suggested that up-regulation of a signaling pathway involving AMPAR-BDNF-TrkB-mTOR might be a common mechanism of psychedelic´s effect on brain plasticity (81). In the case of ketamine, activation of this pathway seems to be related to altered glutamatergic transmission resulting from its antagonism towards the NMDA receptor (81). The modulation of the AMPAR-BDNF-TrkB-mTOR pathway has been less characterized following ibogaine administration. However, the fact that ibogaine too is an NMDA antagonist and can alter neuronal excitability in the cortex (24, 82-84), suggests this pathway as a plausible mechanism of action also for ibogaine.

Another line of evidence suggests that psychedelics induce a heightened sensitivity to BDNF through allosteric modulation of the TrkB receptor (Moliner et al., 2023). While no evidence exists to support this mechanism for ibogaine, atomistic molecular dynamics simulations might be useful to study it (74, 77).

Another limitation of our study is that, when delivered i.p., ibogaine gets rapidly converted to noribogaine through first-pass liver metabolism by the CYP2D6 enzyme (6). Therefore, in the brain, both molecules can be found simultaneously, making it difficult to identify if the observed effects are due to ibogaine, noribogaine, or both acting at the same time (68). Future studies administering only noribogaine i.p. or using the i.v. route (which avoids first-pass liver metabolism) might help in disambiguating these effects.

Conclusions

In conclusion, we found that a single administration of ibogaine to adult mice renders their visual cortex susceptible to plastic changes that are only found during the critical period of ocular dominance plasticity. This increase in plasticity correlates with a reduction of PNNs surrounding PV neurons, as well as a decrease of the inhibitory synaptic marker vGAT. This shows that increased cortical plasticity can be a mechanism behind ibogaine's long lasting therapeutic effects.

Abbreviations

BDNF, Brain Derived Neurotrophic Factor

BSA, Bovine Serum Albumine

bVC, binocular Visual Cortex

CNN, convolutional neural network

GABA, gamma-aminobutyric acid

GDNF, Glial Derived Neurotrophic Factor

GLMM, Generalized Linear Mixed Model

IBO, ibogaine

L, left

LSD, Lysergic acid diethylamide

MD, Monocular Deprivation

MDD, Major Depressive Disorder

MDMA, Methylenedioxymethamphetamine

NMDA, N-methyl-D-aspartate

OMR, Optomotor Response Test

PBS, Phosphate Buffer Saline

PFA, paraformaldehyde

PNN, Perineuronal Net

PTSD, Post-Traumatic Stress Disorder

PV, Parvalbumin

Px, postanatl day x

R, right

REM, Rapid Eye Movement

RT, Room Temperature

SEM, Standard Error of the Mean

SERT, Serotonin Transporter

TBI, Traumatic Brain Injury

VEH, vehicle

vGAT, vesicular GABA transporter

VMAT2, Vesicular Monoamine Transporter 2

WFA, *Wisteria Floribunda* Lectin

Declarations

Ethics approval and consent to participate: All experiments were performed in accordance with the EC Directive 86/609/EEC for animal experiments (directive from the European Commission of the European Economic Community) and the Uruguayan Research Ethic Committees (protocol approval #1621, ExpFCien 240012-000026-22).

Consent for publication: Not applicable.

Availability of data and materials: All data generated or analyzed during this study are included in this published article and its supplementary information files. Raw data are available from the corresponding author on reasonable request.

Competing interests: The authors declare that they have no competing interests.

Funding: This work was supported by Programa de Desarrollo de las Ciencias Básicas (Pedeciba), Agencia Nacional de Investigación a Innovación (ANII), Comisión Sectorial de Investigación Científica (CSIC, grant #22402230100136UD), and European Union - Next Generation EU, Mission 4 Component 1 CUP E53C24001460006, project TNE - NEUROBRIDGE.

Authors' contributions: A.A. and F.M.R. have contributed to the conception and design of the work, the acquisition, analysis and interpretation of data, and have drafted the work and substantively revised it. F.B. and V.T. have contributed to the acquisition and analysis of data. I.C. has contributed to the conception of the work and interpretation of data, and has drafted the work and substantively revised it. J.M.M. has contributed to the acquisition of data; T.P. has contributed to the conception of the work, to the interpretation of data, and has drafted the work and substantively revised it. All authors have approved the submitted version, and have agreed both to be personally accountable for the author's own contributions and to ensure that questions related to the accuracy or integrity of any part of the work, even ones in which the author was not personally involved, are appropriately investigated, resolved, and the resolution documented in the literature.

Acknowledgments: The authors would like to thank Flavio Zolessi (Facultad de Ciencias, UdelaR, Montevideo, Uruguay) for technical support; José P. Prieto (Facultad de Ciencias, UdelaR, Montevideo, Uruguay) for helping in ibogaine treatments; Jessika Urbanavicius (Instituto de Investigaciones Biológicas Clemente Estable, Montevideo, Uruguay) for discussion; Laura Baroncelli (Institute of Neuroscience, IN-CNR, Pisa, Italy) for assistance with vGAT analysis.

References

1. Nutt D. Psychedelics: The Revolutionary Drugs That Could Change Your Life—A Guide from the Expert. Hachette UK; 2024 Jan 2.
2. Fernandes-Nascimento MH, Weber P, Negrão AB. Efficacy and Safety of LSD in the Treatment of Mental and Substance Use Disorders: A Systematic Review of Randomized Controlled Trials. Psychiatry Research. 2025 Jul 5:116622.
3. Vekhova KA, Namiot ED, Jonsson J, Schiöth HB. Ketamine and Esketamine in Clinical Trials: FDA-Approved and Emerging Indications, Trial Trends With Putative Mechanistic Explanations. Clinical Pharmacology & Therapeutics. 2025 Feb;117(2):374-86.
4. O'Brien S, Nutt D. MDMA-assisted therapy: challenges, clinical trials, and the future of MDMA in treating behavioral disorders. CNS spectrums. 2025 Jan;30(1):e15.
5. Højlund M, Kafali HY, Kırmızı B, Fusar-Poli P, Correll CU, Cortese S, Sabé M, Fiedorowicz J, Saraf G, Zein J, Berk M. Efficacy, all-cause discontinuation, and safety of serotonergic psychedelics and MDMA to treat mental disorders: A living systematic review with meta-analysis. European Neuropsychopharmacology. 2025 Dec 1;101:41-55.
6. Alper KR. Ibogaine: a review. Alkaloids Chem Biol. 2001:56:1-38.
7. Wasko MJ, Witt-Enderby PA, Surratt CK. DARK classics in chemical neuroscience: ibogaine. ACS chemical neuroscience. 2018 Sep 14;9(10):2475-83.
8. Belgers M, Leenaars M, Homberg JR, Ritskes-Hoitinga M, Schellekens AF, Hooijmans CR. Ibogaine and addiction in the animal model, a systematic review and meta-analysis. Translational psychiatry. 2016 May;6(5):e826-.
9. Mash DC, Duque L, Page B, Allen-Ferdinand K. Ibogaine detoxification transitions opioid and cocaine abusers between dependence and abstinence: clinical observations and treatment outcomes. Frontiers in pharmacology. 2018 Jun 5;9:345105.
10. Noller GE, Frampton CM, Yazar-Klosinski B. Ibogaine treatment outcomes for opioid dependence from a twelve-month follow-up observational study. The American journal of drug and alcohol abuse. 2018 Jan 2;44(1):37-46.
11. Brown TK, Alper K. Treatment of opioid use disorder with ibogaine: detoxification and drug use outcomes. The American Journal of Drug and Alcohol Abuse. 2018 Jan 2;44(1):24-36.
12. Malcolm BJ, Polanco M, Barsuglia JP. Changes in withdrawal and craving scores in participants undergoing opioid detoxification utilizing ibogaine. Journal of Psychoactive Drugs. 2018 May 27;50(3):256-65.
13. Köck P, Froelich K, Walter M, Lang U, Dürsteler KM. A systematic literature review of clinical trials and therapeutic applications of ibogaine. Journal of Substance Abuse Treatment. 2022 Jul 1;138:108717.
14. Cherian KN, Keynan JN, Anker L, Faerman A, Brown RE, Shamma A, Keynan O, Coetzee JP, Batail JM, Phillips A, Bassano NJ. Magnesium–ibogaine therapy in veterans with traumatic brain injuries.

Nature medicine. 2024 Feb;30(2):373-81.

15. Davis AK, Barsuglia JP, Windham-Herman AM, Lynch M, Polanco M. Subjective effectiveness of ibogaine treatment for problematic opioid consumption: Short-and long-term outcomes and current psychological functioning. Journal of psychedelic studies. 2017 Nov;1(2):65-73.
16. Davis AK, Xin Y, Sepeda N, Averill LA. Open-label study of consecutive ibogaine and 5-MeO-DMT assisted-therapy for trauma-exposed male Special Operations Forces Veterans: prospective data from a clinical program in Mexico. The American Journal of Drug and Alcohol Abuse. 2023 Sep 3;49(5):587-96.
17. Koenig X, Hilber K. The anti-addiction drug ibogaine and the heart: a delicate relation. Molecules. 2015 Jan 29;20(2):2208-28.
18. Nichols DE. Psychedelics. Pharmacological reviews. 2016 Apr 1;68(2):264-355.
19. Staley JK, Ouyang Q, Pablo J, Hearn WL, Flynn DD, Rothman RB, Rice KC, Mash DC. Pharmacological screen for activities of 12-hydroxyibogamine: a primary metabolite of the indole alkaloid ibogaine. Psychopharmacology. 1996 Jun;127(1):10-8.
20. Helsley S, Fiorella D, Rabin RA, Winter JC. Behavioral and biochemical evidence for a nonessential 5-HT2A component of the ibogaine-induced discriminative stimulus. Pharmacology Biochemistry and Behavior. 1998 Feb 1;59(2):419-25.
21. Kohek M, Ohren M, Hornby P, Alcázar-Córcoles MÁ, Bouso JC. The ibogaine experience: A qualitative study on the acute subjective effects of ibogaine. Anthropology of Consciousness. 2020 Mar;31(1):91-119.
22. González Espejito F, Esteban Rodríguez L, Pedrero Pérez EJ, Dickinson J, Kohek M, Guimaraes dos Santos R, Hallak J, Alcázar-Córcoles MÁ, Morgan BL, Bouso JC. The Ibogaine Experience Scale (IES): Development and psychometric properties of a multidimensional measure of ibogaine's subjective effects. PLoS One. 2025 Oct 13;20(10):e0333296.
23. González J, Cavelli M, Castro-Zaballa S, Mondino A, Tort AB, Rubido N, Carrera I, Torterolo P. EEG gamma band alterations and REM-like traits underpin the acute effect of the atypical psychedelic ibogaine in the rat. ACS Pharmacology & Translational Science. 2021 Jan 11;4(2):517-25.
24. Popik P, Layer RT, Fossom LH, Benveniste M, Geter-Douglass B, Witkin JM, Skolnick P. NMDA antagonist properties of the putative antiaddictive drug, ibogaine. The Journal of pharmacology and experimental therapeutics. 1995 Nov 1;275(2):753-60.
25. Hwu C, Havel V, Westergaard X, Mendieta AM, Serrano IC, Hwu J, Walther D, Lankri D, Selinger TL, He K, Liu R. Deciphering Ibogaine's Matrix Pharmacology: Multiple Transporter Modulation at Serotonin Synapses. bioRxiv. 2025 Mar 10:2025-03.
26. Maillet E, Milon N, Fishback J, Schürer S, Heghinian M, Garamszegi N, Mash D. Noribogaine is a Mixed Agonist/Antagonist Opioid Ligand with Profound Functional Selectivity. The FASEB Journal. 2015 Apr;29:LB505.
27. Gassaway MM, Jacques TL, Kruegel AC, Karpowicz Jr RJ, Li X, Li S, Myer Y, Sames D. Deconstructing the iboga alkaloid skeleton: potentiation of FGF2-induced glial cell line-derived

neurotrophic factor release by a novel compound. ACS Chemical Biology. 2016 Jan 15;11(1):77-87.

28. He DY, McGough NN, Ravindranathan A, Jeanblanc J, Logrip ML, Phamluong K, Janak PH, Ron D. Glial cell line-derived neurotrophic factor mediates the desirable actions of the anti-addiction drug ibogaine against alcohol consumption. Journal of Neuroscience. 2005 Jan 19;25(3):619-28.
29. Marton S, González B, Rodríguez-Bottero S, Miquel E, Martínez-Palma L, Pazos M, Prieto JP, Rodríguez P, Sames D, Seoane G, Scorza C. Ibogaine administration modifies GDNF and BDNF expression in brain regions involved in mesocorticolimbic and nigral dopaminergic circuits. Frontiers in pharmacology. 2019 Mar 5;10:193.
30. Nardou R, Sawyer E, Song YJ, Wilkinson M, Padovan-Hernandez Y, De Deus JL, Wright N, Lama C, Faltin S, Goff LA, Stein-O'Brien GL. Psychedelics reopen the social reward learning critical period. Nature. 2023 Jun 22;618(7966):790-8.
31. Biosca-Brull J, Ona G, Alarcón-Franco L, Colomina MT. A transcriptomic analysis in mice following a single dose of ibogaine identifies new potential therapeutic targets. Translational Psychiatry. 2024 Jan 19;14(1):41.
32. Ly C, Greb AC, Cameron LP, Wong JM, Barragan EV, Wilson PC, Burbach KF, Zarandi SS, Sood A, Paddy MR, Duim WC. Psychedelics promote structural and functional neural plasticity. Cell reports. 2018 Jun 12;23(11):3170-82.
33. Cameron LP, Tombari RJ, Lu J, Pell AJ, Hurley ZQ, Ehinger Y, Vargas MV, McCarroll MN, Taylor JC, Myers-Turnbull D, Liu T. A non-hallucinogenic psychedelic analogue with therapeutic potential. Nature. 2021 Jan 21;589(7842):474-9.
34. Vetencourt JF, Sale A, Viegi A, Baroncelli L, De Pasquale R, F. O'Leary O, Castrén E, Maffei L. The antidepressant fluoxetine restores plasticity in the adult visual cortex. Science. 2008 Apr 18;320(5874):385-8.
35. Grieco SF, Qiao X, Zheng X, Liu Y, Chen L, Zhang H, Yu Z, Gavornik JP, Lai C, Gandhi SP, Holmes TC. Subanesthetic ketamine reactivates adult cortical plasticity to restore vision from amblyopia. Current biology. 2020 Sep 21;30(18):3591-603.
36. Kalogeraki E, Greifzu F, Haack F, Löwel S. Voluntary physical exercise promotes ocular dominance plasticity in adult mouse primary visual cortex. Journal of Neuroscience. 2014 Nov 12;34(46):15476-81.
37. Castrén E, Hen R. Neuronal plasticity and antidepressant actions. Trends in neurosciences. 2013 May 1;36(5):259-67.
38. Rosas-Sánchez GU, Germán-Ponciano LJ, Guillen-Ruiz G, Cueto-Escobedo J, Limón-Vázquez AK, Rodríguez-Landa JF, Soria-Fregozo C. Neuroplasticity and mechanisms of action of acute and chronic treatment with antidepressants in preclinical studies. Biomedicines. 2024 Nov 29;12(12):2744.
39. Lepow L, Morishita H, Yehuda R. Critical period plasticity as a framework for psychedelic-assisted psychotherapy. Frontiers in neuroscience. 2021 Sep 20;15:710004.

40. Mataga N, Mizuguchi Y, Hensch TK. Experience-dependent pruning of dendritic spines in visual cortex by tissue plasminogen activator. Neuron. 2004 Dec 16;44(6):1031-41.
41. Bochner DN, Sapp RW, Adelson JD, Zhang S, Lee H, Djurisic M, Syken J, Dan Y, Shatz CJ. Blocking PirB up-regulates spines and functional synapses to unlock visual cortical plasticity and facilitate recovery from amblyopia. Science translational medicine. 2014 Oct 15;6(258):258ra140-.
42. Bukhari N, Burman PN, Hussein A, Demars MP, Sadahiro M, Brady DM, Tsirka SE, Russo SJ, Morishita H. Unmasking proteolytic activity for adult visual cortex plasticity by the removal of Lynx1. Journal of Neuroscience. 2015 Sep 16;35(37):12693-702.
43. Dapueto A, Hayek E, Acuña A, Pannunzio B, Gomez L, Rossi FM. Modulation of cofilin 1 phosphorylation induces juvenile-like plasticity in the adult mouse visual cortex. bioRxiv. 2025 May 10:2025-05.
44. Djurisic M, Vidal GS, Mann M, Aharon A, Kim T, Ferrao Santos A, Zuo Y, Hübener M, Shatz CJ. PirB regulates a structural substrate for cortical plasticity. Proceedings of the National Academy of Sciences. 2013 Dec 17;110(51):20771-6.
45. Hofer SB, Mrsic-Flogel TD, Bonhoeffer T, Hübener M. Experience leaves a lasting structural trace in cortical circuits. Nature. 2009 Jan 15;457(7227):313-7.
46. Hofer SB, Mrsic-Flogel TD, Bonhoeffer T, Hübener M. Experience leaves a lasting structural trace in cortical circuits. Nature. 2009 Jan 15;457(7227):313-7.
47. Huang Y, Liu Z, Zhan Z, Zhang X, Gao L, Wang M, Fu Y, Huang L, Yu M. Interactions between excitatory neurons and parvalbumin interneurons in V1 underlie neural mechanisms of amblyopia and visual stimulation treatment. Communications Biology. 2024 Nov 25;7(1):1564.
48. Hensch TK. Critical period plasticity in local cortical circuits. Nature reviews neuroscience. 2005 Nov 1;6(11):877-88.
49. Huang ZJ, Kirkwood A, Pizzorusso T, Porciatti V, Morales B, Bear MF, Maffei L, Tonegawa S. BDNF regulates the maturation of inhibition and the critical period of plasticity in mouse visual cortex. Cell. 1999 Sep 17;98(6):739-55.
50. Harauzov A, Spolidoro M, DiCristo G, De Pasquale R, Cancedda L, Pizzorusso T, Viegi A, Berardi N, Maffei L. Reducing intracortical inhibition in the adult visual cortex promotes ocular dominance plasticity. Journal of Neuroscience. 2010 Jan 6;30(1):361-71.
51. Harauzov A, Spolidoro M, DiCristo G, De Pasquale R, Cancedda L, Pizzorusso T, Viegi A, Berardi N, Maffei L. Reducing intracortical inhibition in the adult visual cortex promotes ocular dominance plasticity. Journal of Neuroscience. 2010 Jan 6;30(1):361-71.
52. Chaudhry FA, Reimer RJ, Bellocchio EE, Danbolt NC, Osen KK, Edwards RH, Storm-Mathisen J. The vesicular GABA transporter, VGAT, localizes to synaptic vesicles in sets of glycinergic as well as GABAergic neurons. Journal of Neuroscience. 1998 Dec 1;18(23):9733-50.
53. Pizzorusso T, Medini P, Berardi N, Chierzi S, Fawcett JW, Maffei L. Reactivation of ocular dominance plasticity in the adult visual cortex. Science. 2002 Nov 8;298(5596):1248-51.

54. Fawcett JW, Oohashi T, Pizzorusso T. The roles of perineuronal nets and the perinodal extracellular matrix in neuronal function. Nature Reviews Neuroscience. 2019 Aug;20(8):451-65.
55. Donato F, Rompani SB, Caroni P. Parvalbumin-expressing basket-cell network plasticity induced by experience regulates adult learning. Nature. 2013 Dec 12;504(7479):272-6.
56. Kuhlman SJ, Olivas ND, Tring E, Ikrar T, Xu X, Trachtenberg JT. A disinhibitory microcircuit initiates critical-period plasticity in the visual cortex. Nature. 2013 Sep 26;501(7468):543-6.
57. Cisneros-Franco JM, de Villers-Sidani É. Reactivation of critical period plasticity in adult auditory cortex through chemogenetic silencing of parvalbumin-positive interneurons. Proceedings of the National Academy of Sciences. 2019 Dec 26;116(52):26329-31.
58. González B, Fagundez C, Peixoto de Abreu Lima A, Suescun L, Sellanes D, Seoane GA, Carrera I. Efficient access to the iboga skeleton: optimized procedure to obtain voacangine from Voacanga africana root bark. ACS omega. 2021 Jun 24;6(26):16755-62.
59. Prusky GT, Alam NM, Beekman S, Douglas RM. Rapid quantification of adult and developing mouse spatial vision using a virtual optomotor system. Investigative ophthalmology & visual science. 2004 Dec 1;45(12):4611-6.
60. Douglas RM, Alam NM, Silver BD, McGill TJ, Tschetter WW, Prusky GT. Independent visual threshold measurements in the two eyes of freely moving rats and mice using a virtual-reality optokinetic system. Visual neuroscience. 2005 Sep;22(5):677-84.
61. Peirce J, MacAskill M, Hirst R. Building experiments in PsychoPy. 2022. Sage Publications.
62. Keith BJ, Franklin GP, Paxinos G. The mouse brain in stereotaxic coordinates. California: Academic. 2008.
63. Braak H, Braak E. Golgi preparations as a tool in neuropathology with particular reference to investigations of the human telencephalic cortex. Progress in neurobiology. 1985 Jan 1;25(2):93-139.
64. Spruston N. Pyramidal neurons: dendritic structure and synaptic integration. Nature Reviews Neuroscience. 2008 Mar;9(3):206-21.
65. Faraway, J. J. Extending the linear model with R: generalized linear, mixed effects and nonparametric regression models. 2016. Chapman and Hall/CRC.
66. Bates D, Mächler M, Bolker B, Walker S (2015). “Fitting Linear Mixed-Effects Models Using lme4.” Journal of Statistical Software, 67(1), 1–48. doi:10.18637/jss.v067.i01.
67. Fox J, Weisberg S. An R companion to applied regression. Sage publications; 2018 Sep 27.
68. Rodríguez P, Urbanavicius J, Prieto JP, Fabius S, Reyes AL, Havel V, Sames D, Scorza C, Carrera I. A single administration of the atypical psychedelic ibogaine or its metabolite noribogaine induces an antidepressant-like effect in rats. ACS Chemical Neuroscience. 2020 Apr 24;11(11):1661-72.
69. Tropea D, Van Wart A, Sur M. Molecular mechanisms of experience-dependent plasticity in visual cortex. Philosophical Transactions of the Royal Society B: Biological Sciences. 2009 Feb 12;364(1515):341-55.

70. Lensjø KK, Lepperød ME, Dick G, Hafting T, Fyhn M. Removal of perineuronal nets unlocks juvenile plasticity through network mechanisms of decreased inhibition and increased gamma activity. Journal of Neuroscience. 2017 Feb 1;37(5):1269-83.
71. Wingert JC, Sorg BA. Impact of perineuronal nets on electrophysiology of parvalbumin interneurons, principal neurons, and brain oscillations: a review. Frontiers in synaptic neuroscience. 2021 May 10;13:673210.
72. Mainardi M, Scabia G, Vottari T, Santini F, Pinchera A, Maffei L, Pizzorusso T, Maffei M. A sensitive period for environmental regulation of eating behavior and leptin sensitivity. Proceedings of the National Academy of Sciences. 2010 Sep 21;107(38):16673-8.
73. Vierci G, Pannunzio B, Bornia N, Rossi FM. H3 and H4 lysine acetylation correlates with developmental and experimentally induced adult experience-dependent plasticity in the mouse visual cortex: supplementary issue: Brain plasticity and repair. Journal of experimental neuroscience. 2016 Jan;10:JEN-S39888.
74. Cannarozzo C, Rubiolo A, Casarotto P, Castrén E. Ketamine and its metabolite 2 R, 6 R-hydroxynorketamine promote ocular dominance plasticity and release tropomyosin-related kinase B from inhibitory control without reducing perineuronal nets enwrapping parvalbumin interneurons. European Journal of Neuroscience. 2023 Mar;57(6):940-50.
75. Casarotto PC, Girych M, Fred SM, Kovaleva V, Moliner R, Enkavi G, Biojone C, Cannarozzo C, Sahu MP, Kaurinkoski K, Brunello CA. Antidepressant drugs act by directly binding to TRKB neurotrophin receptors. Cell. 2021 Mar 4;184(5):1299-313.
76. Venturino A, Schulz R, De Jesús-Cortés H, Maes ME, Nagy B, Reilly-Andújar F, Colombo G, Cubero RJ, Uiterkamp FE, Bear MF, Siegert S. Microglia enable mature perineuronal nets disassembly upon anesthetic ketamine exposure or 60-Hz light entrainment in the healthy brain. Cell reports. 2021 Jul 6;36(1).
77. Moliner R, Girych M, Brunello CA, Kovaleva V, Biojone C, Enkavi G, Antenucci L, Kot EF, Goncharuk SA, Kaurinkoski K, Kuutti M. Psychedelics promote plasticity by directly binding to BDNF receptor TrkB. Nature Neuroscience. 2023 Jun;26(6):1032-41.
78. Hsiao Y, Fonseca MA, Tiemroth AS, Vasquez EJ, Gomez AM. Persistent large-scale changes in alternative splicing in prefrontal cortical neuron types following psychedelic exposure. bioRxiv. 2025 Jan 16:2025-01.
79. Liao C, O'Farrell E, Qalieh Y, Savalia NK, Girgenti MJ, Kwan KY, Kwan AC. Single-nucleus transcriptomics reveals time-dependent and cell-type-specific effects of psilocybin on gene expression. bioRxiv. 2025 Jan 4.
80. Tiwari P, Davoudian PA, Kapri D, Vuruputuri RM, Karaba LA, Sharma M, Zanni G, Balakrishnan A, Chaudhari PR, Pradhan A, Suryavanshi S. Ventral hippocampal parvalbumin interneurons gate the acute anxiolytic action of the serotonergic psychedelic DOI. Neuron. 2024 Nov 20;112(22):3697-714.
81. Agnorelli C, Spriggs M, Godfrey K, Sawicka G, Bohl B, Douglass H, Fagiolini A, Parastoo H, Carhart-Harris R, Nutt D, Erritzoe D. Neuroplasticity and psychedelics: A comprehensive examination of

classic and non-classic compounds in pre and clinical models. Neuroscience & Biobehavioral Reviews. 2025 Apr 2:106132.

82. González J, Prieto JP, Rodríguez P, Cavelli M, Benedetto L, Mondino A, Pazos M, Seoane G, Carrera I, Scorza C, Torterolo P. Ibogaine acute administration in rats promotes wakefulness, long-lasting REM sleep suppression, and a distinctive motor profile. Frontiers in pharmacology. 2018 Apr 27;9:374.
83. González J, Cavelli M, Castro-Zaballa S, Mondino A, Tort AB, Rubido N, Carrera I, Torterolo P. EEG gamma band alterations and REM-like traits underpin the acute effect of the atypical psychedelic ibogaine in the rat. ACS Pharmacology & Translational Science. 2021 Jan 11;4(2):517-25.
84. Villalba S, Bosch S, Di Constanzo L, González B, Torterolo P, Carrera I, Urbano FJ, Bisagno V. Noribogaine altered intrinsic properties of thalamocortical neurons in a sex-dependent manner. Progress in Neuro-Psychopharmacology and Biological Psychiatry. 2025 Aug 9:111467.

Figures

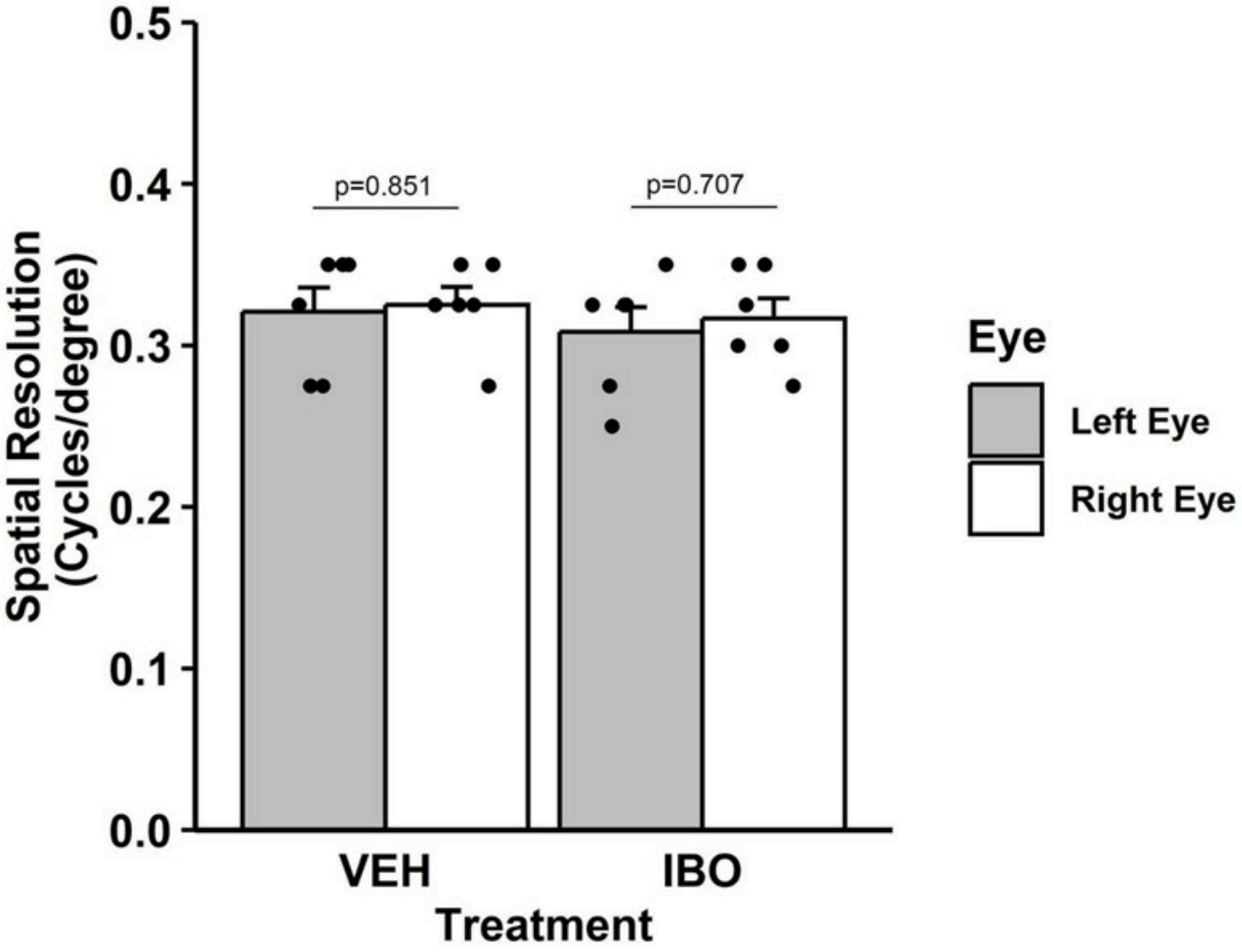

Figure 1

Visual acuity is not affected by ibogaine treatment in adult mice. The graph shows the maximal spatial frequency (c/d) detected through the left (L, grey bars) and right (R, white bars) eye of vehicle (VEH) and ibogaine (IBO) treated adult mice. Data are expressed as mean spatial frequency±SEM, and each black dot represents one animal. No difference was detected between treatments (χ^2_1=0.004, p=0.948) nor between the left and right eye of vehicle-treated and of ibogaine-treated mice (VEH L: 0.308±0.015 vs. VEH R: 0.325±0.011, n=6, t_{26}=-0.190, p=0.851; IBO L: 0.320±0.015 vs. IBO R: 0.316±0.012, n=6, t_{26}=-0.379, p=0.707).

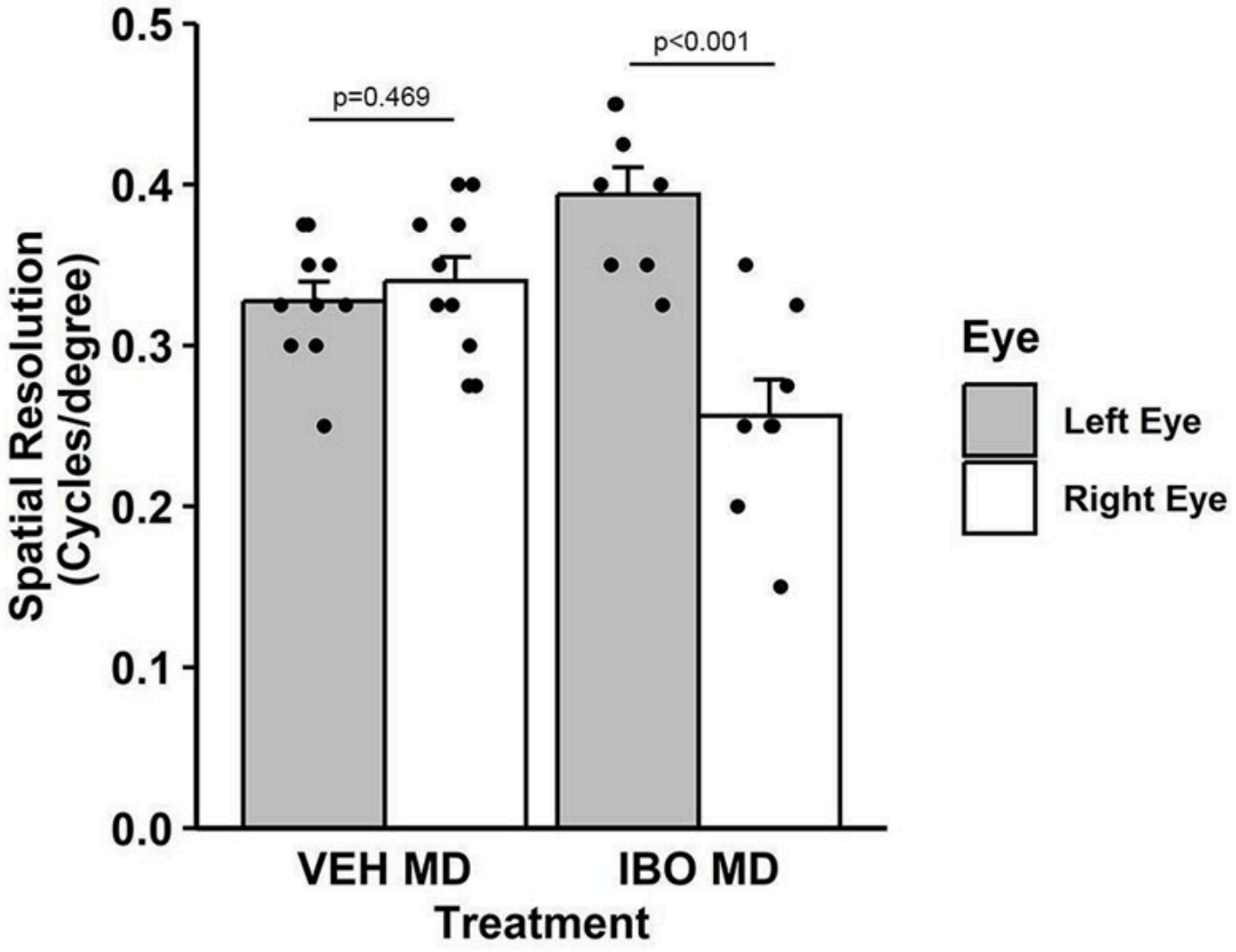

Figure 2

Ibogaine induces functional plasticity in adult mice. The graph shows the maximal spatial frequency (c/d) detected through the left (L, grey bars) and right deprived (R, white bars) eye of vehicle (VEH) and ibogaine (IBO) treated adult mice. Data are expressed as mean spatial frequency±SEM, and each black dot represents one animal. No difference was detected between left and right deprived eye in vehicle-treated adult mice (VEH L: 0.327±0.012 vs. VEH R: 0.340±0.015, n=10, t_{26}=-0.734, p=0.469). On the

contrary, in ibogaine treated mice, visual acuity of MD eye was reduced in comparison to the right un-deprived eye (IBO L: 0.393±0.016 vs. IBO R: 0.256±0.022, n=8, t_{26}=7.221, p< 0.001).

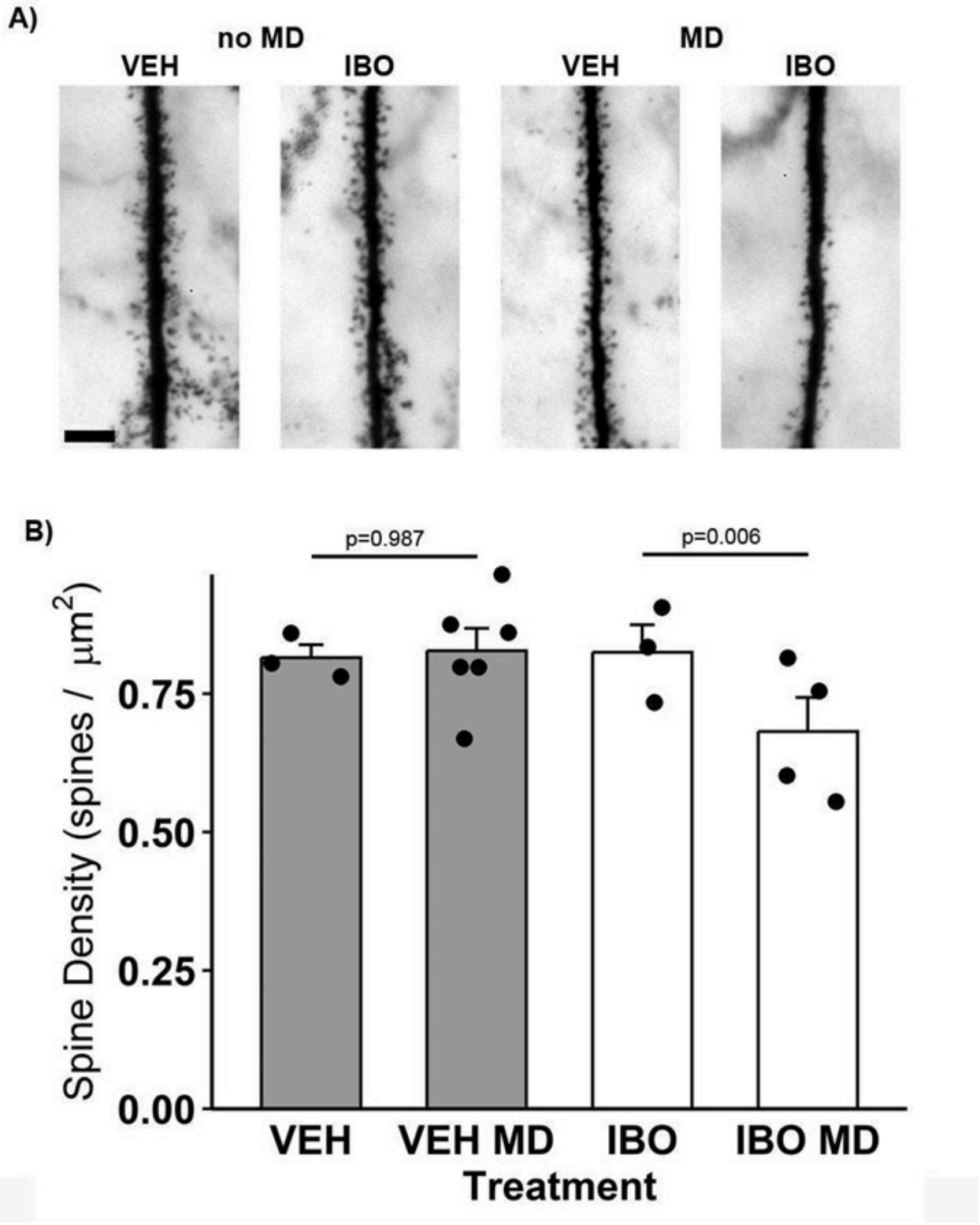

Figure 3

Ibogaine induces structural plasticity in adult mice. A) Representative images of apical dendrites of the left (contralateral) visual cortex of un-deprived and deprived (MD) adult mice treated with vehicle (VEH) or ibogaine (IBO). Bar: 5 µm. B) The graph shows the dendritic spine density (spines/µm) of the left

(contralateral) visual cortex of un-deprived and deprived (MD) adult mice treated with vehicle (VEH) or ibogaine (IBO). Data are expressed as mean dendritic spine density±SEM, and each black dot represents one dendrite. No difference was detected between vehicle- and ibogaine-treated un-deprived mice (IBO: 0.825±0.049, n=13 dendrites, n=3, vs.VEH: 0.815±0.023, n=19 dendrites, n=3, vs. z=0,331, p=0.987). On the contrary, MD reduced dendritic spine density in ibogaine-treated vs. vehicle treated adult mice (IBO MD: 0.681±0.061, n=14 dendrites, n=4, vs. VEH MD: 0.827±0.040, n=32 dendrites, n=6, z=-2.743, p=0.006).

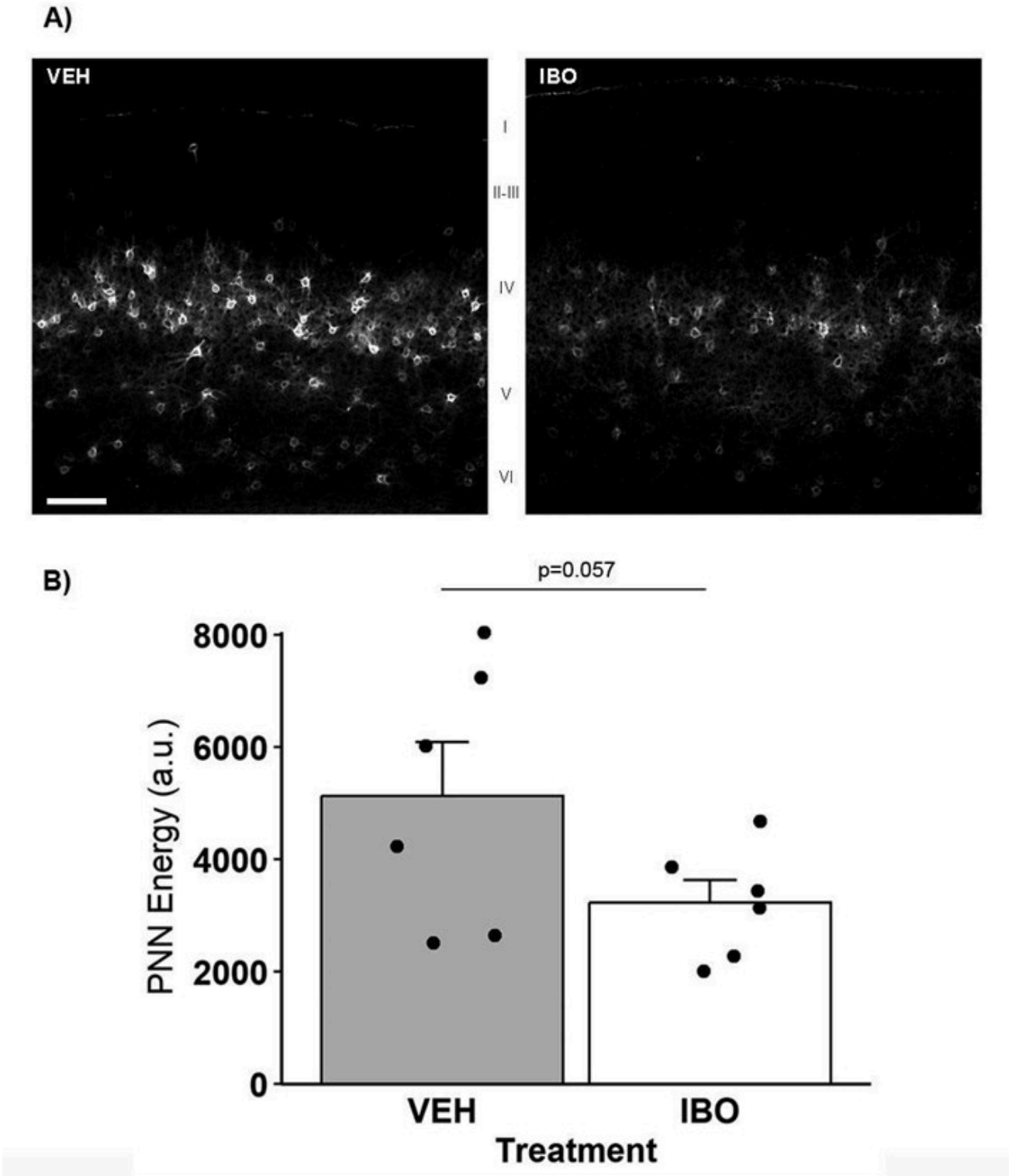

Figure 4

Ibogaine induces a reduction of PNN energy in the visual cortex of adult mice. A) Representative images of WFA-stained 50 µm sections of the visual cortex of adult mice treated with vehicle (VEH) or ibogaine (IBO). Bar=150 µm. Cortical layers are indicated. B) The graph shows the PNN energy (a.u.) of the visual cortex of VEH (grey bar) and IBO (white bar) adult mice. Data are expressed as mean PNN energy±SEM, and each black dot represents one animal. Ibogaine induces a decrease of PNN energy in ibogaine-treated vs. vehicle treated adult mice (IBO: 3220.410±3.902 (a.u.), n=6, vs. VEH: 5119.520±960.337 (a.u.), n=6, χ^2_1=-3.599, p=0.057).

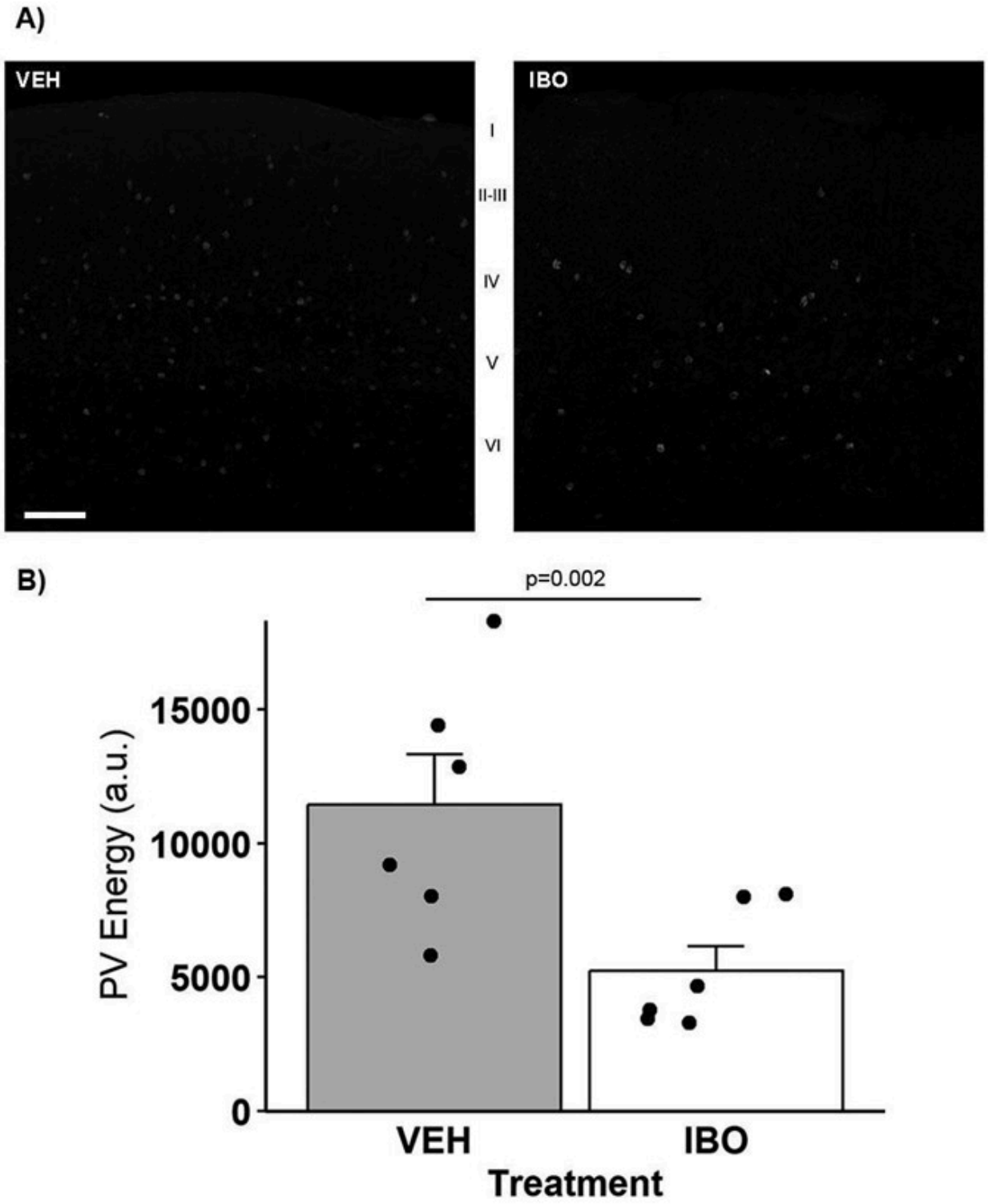

Figure 5

Ibogaine induces a reduction of PV energy in the visual cortex of adult mice. A) Representative images of PV-stained 50 µm sections of the visual cortex of adult mice treated with vehicle (VEH) or ibogaine (IBO). Bar=150 µm. Cortical layers are indicated. B) The graph shows the PV energy (a.u.) of the visual cortex of VEH (grey bar) and IBO (white bar) adult mice. Data are expressed as mean PV energy±SEM, and each black dot represents one animal. PV energy decreases in ibogaine-treated vs. vehicle treated

adult mice (VEH: 11437.911±1882.036 (a.u.), n=6, vs. IBO: 5222.456±915.487 (a.u.), n=6, χ^2_1=9.087, p=0.002).

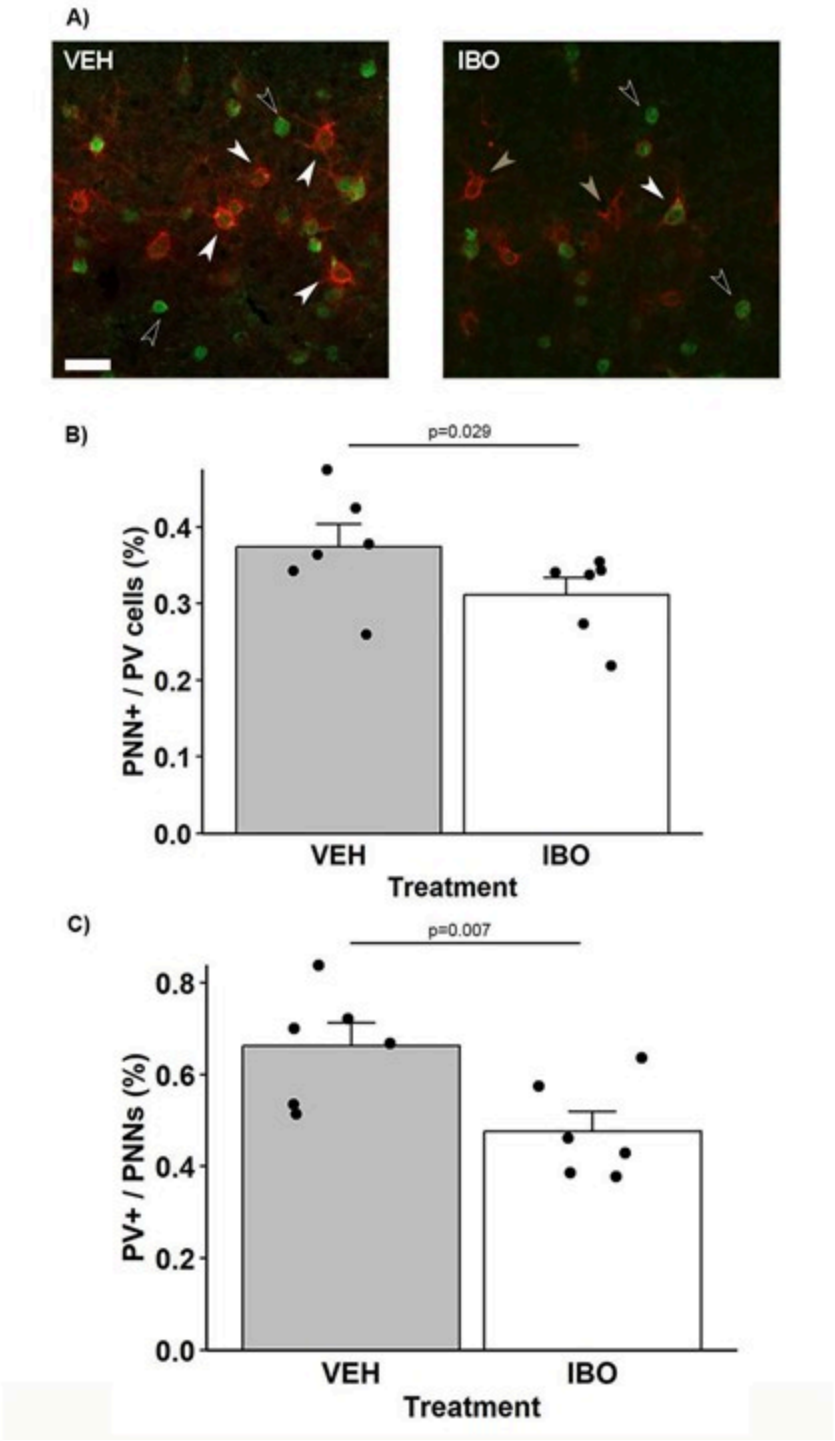

Figure 6

Ibogaine reduces the percentage of PNNS/PVs colocalized structures in the visual cortex of adult mice. A) Representative images of PNN (red) / PV (green)-stained 50 µm sections of the visual cortex of adult mice treated with vehicle (VEH) or ibogaine (IBO). Bar=50 µm. Arrows indicate PV+ only cells (black), PNN+ only structures (grey), and PV+/PNN+ structures (white). B) The graphs show the percentage of

PVs surrounded by PNNs (PNN+/PVs cells, left) and the percentage of PNNs surrounding PV cells (PV+/PNNs, right) in the visual cortex of VEH (grey bar) and IBO (white bar) adult mice. Data are expressed as mean % of co-localization±SEM, and each black dot represents one animal. PNN+/PV cells: VEH: 31.178.±2.198%, n=6, vs. IBO: 37.431±2.992%, n=6, χ^2_1=4.739, p=0.029; PV+/PNNs: VEH: 66.326.±4.907%, n=6, vs. IBO: 47.665±4.723%, n=6, χ^2_1=7.146, p=0.007.

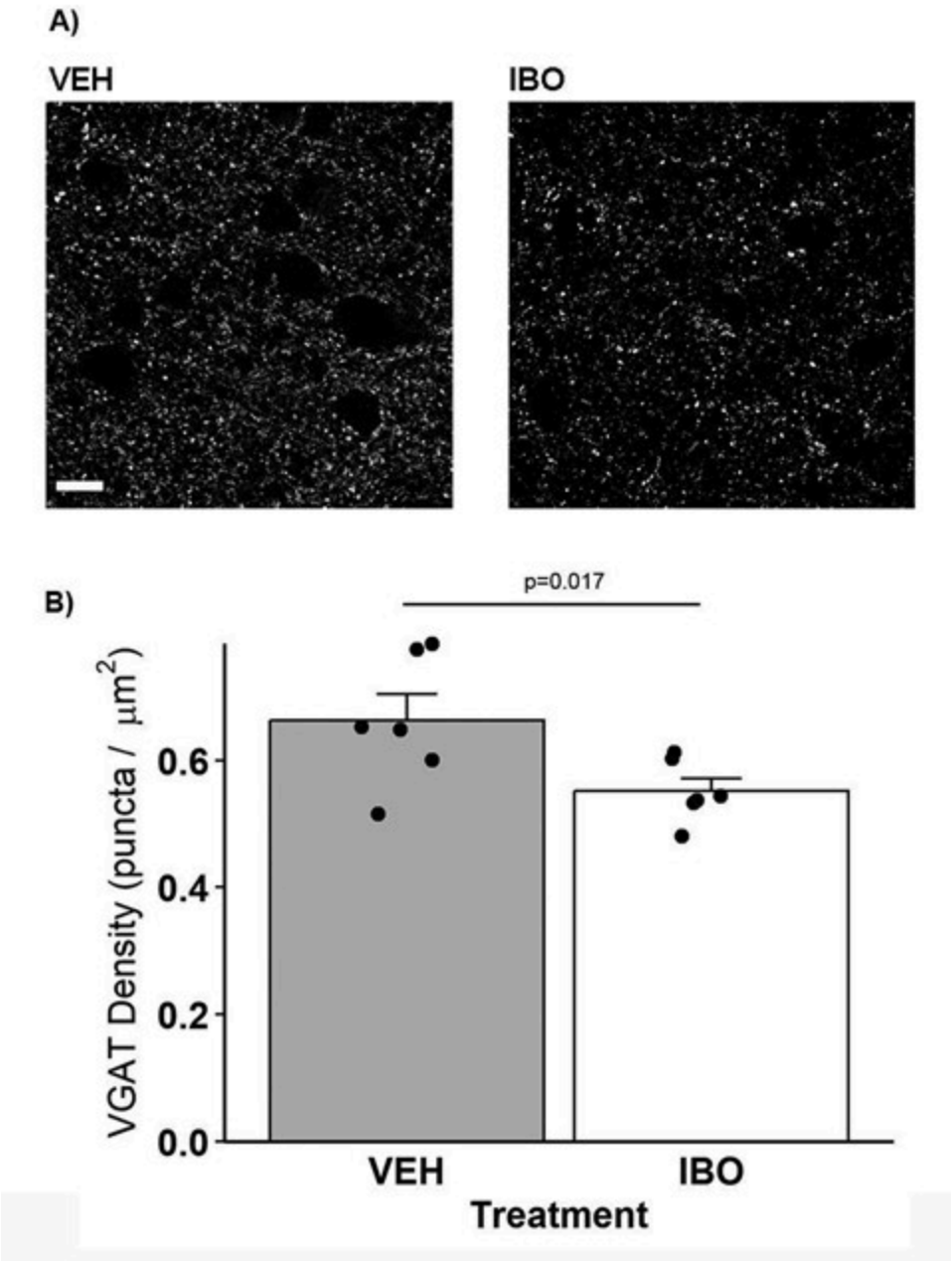

Figure 7

Ibogaine reduces vGAT staining in the visual cortex of adult mice. A) Representative images of vGAT-stained 50 µm sections of the visual cortex of adult mice treated with vehicle (VEH) or ibogaine (IBO). Bar=10 µm. B) The graph shows the density of vGAT-positive puncta (puncta/µm^2) of the visual cortex of VEH (grey bar) and IBO (white bar) adult mice. Data are expressed as mean vGAT density±SEM, and each black dot represents one animal. VEH: 0.657±0.039, n=6, vs. IBO: 0.552±0.020, n=6, χ^2_1=5.644, p=0.017.

Supplementary Files

This is a list of supplementary files associated with this preprint. Click to download.

- SUPPLEMENTARYMATERIALACUABMC.doc